

Switched Control Applied to a Totem-Pole Bridgeless Rectifier for Power Factor Correction

Luan Vinícius Fiorio

Department of Electrical Engineering
Santa Catarina State University
Joinville, Brazil
luan.lvf@edu.udesc.br

Tiago Jackson May Dezuo

Department of Electrical Engineering
Santa Catarina State University
Joinville, Brazil
tiago.dezuo@udesc.br

Yales Rômulo de Novaes

Department of Electrical Engineering
Santa Catarina State University
Joinville, Brazil
yales.novaes@udesc.br

Abstract—The wide range of operation of bridgeless rectifiers requires a control technique that guarantee robustness. Linear Power Factor Correction (PFC) control techniques, although effective, cannot guarantee such robustness. Nonlinear techniques such as one cycle control are more robust, but other options should be explored. In this work, an affine model is obtained for a Totem-Pole Bridgeless Rectifier (TPBR). An extension to an existing switched control design technique is presented in order to achieve PFC in a robust fashion for the TPBR. Simulations with nonideal components and distorted grid voltage show a precise, fast and robust performance of the switched controller. The effective reference following of the proposed method allows the user to define a current reference waveform that prioritize THD or power factor, depending on the application and norm requirements.

Index Terms—Switched Control, Totem-Pole Bridgeless Rectifier, Power Factor Correction, Robust

I. INTRODUCTION

Bridgeless rectifiers, as the Totem-Pole Bridgeless Rectifier (TPBR) [1], can achieve higher efficiency than the conventional Boost converter and are able to reduce conduction losses. The limitation in those topologies were given by the semiconductor technology [2], mainly the reverse recovery of body diodes of the MOSFETs. With the increase of semiconductors research and products, high-performance silicon Insulated-Gate Bipolar Transistor IGBT [3], wide bandgap semiconductors like Silicon Carbide (SiC) [3], [4] and Gallium Nitride (GaN) [3], [5] have allowed the TPBR to achieve high efficiency in practice, up to 99 %.

Possible control strategies that are able to control the TPBR with power factor correction for the input current are: Average-Analog (A-A) [6], Digital-Average (D-A) [7], Trailing-Edge Modulated One Cycle Control (TEM-OCC) [8], [9], Digital-Peak Current (D-PC) [3], Leading-Edge Modulated OCC (LEM-OCC) [8], LEM-OCC Stability and Distortion (LEM-OCC-SD) [10], and LEM-OCC-SD Simplified (LEM-OCC-SDS) [10]. The OCC-based methods have shown to be more robust than the previously cited techniques, which is expected from its nonlinear nature.

The authors thanks Fundação de Amparo à Pesquisa e Inovação do Estado de Santa Catarina (FAPESC) - Grant number 288/2021 for the financial support.

Another nonlinear approach that could achieve high power factor is Switched Control [11], [12]. As the TPBR can be modeled as an affine¹ switched system, a switching rule design [13], [14] can be obtained in order to stabilize the process that guarantees Lyapunov-based stability for all designed operation range, which presents stronger theoretical robustness guarantees than OCC-based approaches for any uncertain parameter varying inside a polytope region [15]. The switching control can also be extended to include optimization objectives, as the \mathcal{H}_∞ method for minimizing the effects of disturbance [16]. As the switched control laws are designed in an offline fashion, its application can be done with a digital signal processor with low computational complexity.

This paper presents the application of a switching rule to a Totem-Pole Bridgeless Rectifier operating in Continuous Conduction Mode (CCM) with the objective of stabilization and power factor correction. Extensions are made to the design procedure of the switching rule to allow power factor correction. Section II presents the modeling of the TPBR as a switched system, as well as a brief review over the existing Power Factor Correction (PFC) control techniques. Section III reviews the switching rule design considering the switched control approach for affine systems as presented in [14], whilst Section IV extends the existing design procedure to achieve a high power factor over rectifier type of converters. Finally, Section V presents the obtained nonideal simulation results and Section VI concludes this work.

II. THE TOTEM-POLE BRIDGELESS RECTIFIER

The Totem-Pole Bridgeless Rectifier (Fig. 1) is an AC-DC converter with a totem-pole arm of transistors in the rectifier bridge. The converter is based on the full-bridge diode rectifier with capacitive filter but it uses switches in the place of two diodes, which has the potential to reduce conduction losses and allows the designer to achieve high power factor using a PFC control technique [2].

The modes of operation for the TPBR rely directly on the sign of the input voltage and are presented in Table I. At the first mode, the current flows through the S_2 and D_2 , with the output voltage v_{C_o} being held by the energy stored in capacitor

¹Nonlinear systems that are linear in the input.

TABLE I: Modes of operation of the TPBR.

Mode	S_1 state	S_2 state	v_{in} sign
1	OFF	ON	> 0
2	OFF	OFF	> 0
3	ON	OFF	< 0
4	OFF	OFF	< 0

C_o . With the command to block S_2 , the second mode begins, but the current now flows through D_2 and the intrinsic diode of S_1 to the output capacitor and load. The third and fourth modes follows the same behavior, analogously. The described operation regards CCM operation, and it used as base for the affine model design in next section.

A. Affine model

The system can be represented in a nonlinear fashion by considering the state-space affine model [14]

$$\dot{x}(t) = A_i x(t) + b_i, \quad i \in \mathcal{M} := \{1, \dots, m\}, \quad (1)$$

where $x \in \mathbb{R}^n$ are the states with its derivatives $\dot{x}(t)$, $A_i \in \mathbb{R}^{n \times n}$, $b_i \in \mathbb{R}$, are the matrices for each mode $i \in \mathcal{M}$ of the system.

Considering $x = [i_{L_B} \ v_{C_o}]'$ as the state vector of the TPBR, the expressions for its model in CCM can be obtained as follows: for Mode 1, a mesh with the inductor L_B , the conducting switch S_2 , the diode D_2 and the input voltage source v_{in} results in the differential equation

$$\frac{di_{L_B}}{dt} = -i_{L_B} \frac{R_B}{L_B} + v_{in} \frac{1}{L_B}, \quad (2)$$

where R_B is the inductor's resistance. Also, a node at the output capacitor C_o and the load resistance R_L results in

$$\frac{dv_{C_o}}{dt} = -v_{C_o} \frac{1}{R_L C_o}. \quad (3)$$

Nevertheless, resulting in the state-space matrices for the first mode:

$$A_1 = \begin{bmatrix} -\frac{R_B}{L_B} & 0 \\ 0 & -\frac{1}{R_L C_o} \end{bmatrix}, \quad b_1 = \begin{bmatrix} \frac{v_{in}}{L_B} \\ 0 \end{bmatrix}. \quad (4)$$

In Mode 2, the current flows through diode D_2 and the intrinsic diode of switch S_1 to the output capacitor and load, which gives

$$\frac{di_{L_B}}{dt} = -i_{L_B} \frac{R_B}{L_B} - v_{C_o} \frac{1}{L_B} + v_{in} \frac{1}{L_B}, \quad (5)$$

and

$$\frac{dv_{C_o}}{dt} = i_{L_B} \frac{1}{C_o} - v_{C_o} \frac{1}{R_L C_o}, \quad (6)$$

being represented as

$$A_2 = \begin{bmatrix} -\frac{R_B}{L_B} & -\frac{1}{L_B} \\ \frac{1}{C_o} & -\frac{1}{R_L C_o} \end{bmatrix}, \quad b_2 = \begin{bmatrix} \frac{v_{in}}{L_B} \\ 0 \end{bmatrix}. \quad (7)$$

During Mode 3, the input current flows through the switch S_1 and the diode D_1 . The output voltage v_o is held steady by

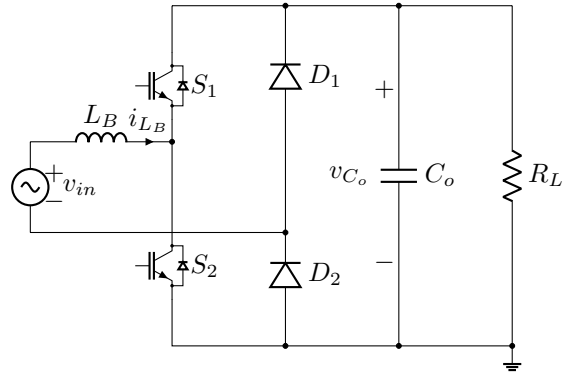


Fig. 1: Totem-pole Bridgeless Rectifier.

the output capacitor C_o , subject to its ripple. This operation can be translated to the expressions

$$\frac{di_{L_B}}{dt} = -i_{L_B} \frac{R_B}{L_B} + v_{in} \frac{1}{L_B}, \quad (8)$$

and

$$\frac{dv_{C_o}}{dt} = -v_{C_o} \frac{1}{R_L C_o}, \quad (9)$$

resulting in the state matrices

$$A_3 = \begin{bmatrix} -\frac{R_B}{L_B} & 0 \\ 0 & -\frac{1}{R_L C_o} \end{bmatrix}, \quad b_3 = \begin{bmatrix} \frac{v_{in}}{L_B} \\ 0 \end{bmatrix}. \quad (10)$$

Mode 4, similarly to Mode 2, occurs when both switches are in OFF-state and the current flows through the intrinsic diode of S_2 and diode D_1 to the output capacitor C_o and load R_L . The expressions that describe this behavior are

$$\frac{di_{L_B}}{dt} = -i_{L_B} \frac{R_B}{L_B} + v_{C_o} \frac{1}{L_B} + v_{in} \frac{1}{L_B}, \quad (11)$$

and

$$\frac{dv_{C_o}}{dt} = -i_{L_B} \frac{1}{C_o} - v_{C_o} \frac{1}{R_L C_o}, \quad (12)$$

resulting in

$$A_4 = \begin{bmatrix} -\frac{R_B}{L_B} & \frac{1}{L_B} \\ -\frac{1}{C_o} & -\frac{1}{R_L C_o} \end{bmatrix}, \quad b_4 = \begin{bmatrix} \frac{v_{in}}{L_B} \\ 0 \end{bmatrix}. \quad (13)$$

B. Control strategies for power factor correction

Average-Analog aims to control average values, which can result in satisfactory THD under light load operation, but the average nature makes the control slower and less precise. Digital-Average uses rising edge sampling [17] to sense the input current during switch ON time. D-A control results in increased THD during Discontinuous Conduction Mode (DCM) operation. Trailing-Edge Modulated One Cycle Control controls the peak input current indirectly, by directly controlling the OFF-time of the switches. The input current's THD is higher than Average-Analog control [18]. Digital-Peak Current samples the peak of the inductor's current, resulting in high THD when the input current's ripple is high.

The Leading-Edge Modulated One Cycle Control technique, differently from the D-PC, controls the ON-time of

the switches. For light load, results present high total harmonic distortion and stability problems with low voltage gain. LEM-OCC Stability and Distortion and its simplified version are both able to control the ON-time of the switches with lower THD than the previous presented techniques and better stability results [10]. The THD for the LEM-OCC-SD is theoretically zero, although the generation of fictitious current in practice limits its THD, resulting in low but not zero values. LEM-OCC-SDS allows the use of analog circuits to implement the technique.

A technique that presents stronger theoretical robustness than the previous commented techniques is switched control, since it guarantees Lyapunov-based stability for all designed operation range. From its switched nature, faster and more precise responses are expected than other control techniques, since the technique decides at which mode to operate based on the instantaneous value of the states, not on its mean value. The result of the controller is an operation mode, not a duty cycle value, which naturally avoids saturation. Also, as the system is modeled as a switched (affine) system, the differences between simulated results and real-world results are reduced. The switched control technique for affine systems is presented in the next section.

III. SWITCHED CONTROL FOR AFFINE SYSTEMS

Considering the affine system with dynamics defined by (1), a switching rule can be designed with the goal of driving the system state to a given constant equilibrium point x_{eq} . Given the tracking error dynamics

$$\dot{e}(t) = A_i e(t) + k_i, \quad (14a)$$

$$k_i = b_i + A_i x_{eq}, \quad (14b)$$

$$e(t) := x(t) - x_{eq}, \quad (14c)$$

a switching rule can be defined as [14]

$$\sigma(e(t)) = \arg \max_{i \in \mathcal{M}} \{v_i(e(t))\}, \quad (15a)$$

$$v_i(e(t)) = e(t)' P_i e(t) + 2e(t)' S_i, \quad (15b)$$

where $P_i = P'_i \in \mathbb{R}^{n \times n}$ and $S_i \in \mathbb{R}^n$ are the variables of decision, which need to be determined. Fig. 2 shows the block diagram for the switched control technique according to the aforementioned expressions. Sliding mode dynamics may occur in any switching surface and can be represented by

$$\dot{e}(t) = \sum_{i=1}^m \theta_i(e(t)) (A_i e(t) + k_i), \quad \theta(e(t)) \in \Theta, \quad (16)$$

where Θ is the unitary simplex and $\theta_i(e(t)) = 0$ if $i \notin \sigma(e(t))$.

From the main results obtained in [14], it is supposed that $\exists P, S, L$ solving the Linear Matrix Inequality (LMI) problem

$$\begin{cases} \bar{P} = \sum_{i=1}^m \bar{\theta}_i P_i > 0; \\ \bar{S} = \sum_{i=1}^m \bar{\theta}_i S_i = 0; \\ Q'_a (\Psi + \Phi + LC_b(\theta) + C_b(\theta)' L') Q_a < 0, \end{cases} \quad (17)$$

where

$$\Psi = \begin{bmatrix} A'P + P'A - \alpha' \bar{P} I_a - I'_a \bar{P} \alpha & \bullet \\ K'P + S'A & K'S + S'K \end{bmatrix}, \quad (18a)$$

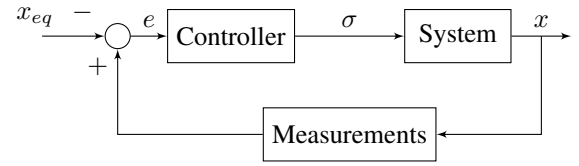


Fig. 2: Control block diagram for the switched control technique.

$$\Phi = \begin{bmatrix} \alpha'(P - \bar{P}I_a) + (P' - I'_a \bar{P})\alpha & \bullet \\ 2S'\alpha & 0_{m \times m} \end{bmatrix}, \quad (18b)$$

with

$$A = [A_1 \dots A_m]; \quad K = [k_1 \dots k_m], \quad (19a)$$

$$P = [P_1 \dots P_m]; \quad S = [S_1 \dots S_m], \quad (19b)$$

$$\alpha = [\alpha_1 I_n \dots \alpha_m I_n]; \quad I_a = \mathbf{1}_m \otimes I_n, \quad (19c)$$

$$\mathbf{1}_m = [1 \dots 1] \in \mathbb{R}^m; \quad C_a = [0_{1 \times mn} \quad \mathbf{1}_m], \quad (19d)$$

$$C_b(\theta) = \begin{bmatrix} \aleph_\theta \otimes I_n & 0_{rn \times m} \\ 0_{r \times m} & \aleph_\theta - \aleph_{\bar{\theta}} \end{bmatrix}, \quad (19e)$$

in which $\bar{\theta}$ is a constant scalar such that

$$\sum_{i=1}^m \bar{\theta}_i k_i = 0 \quad \sum_{i=1}^m \bar{\theta}_i = 1, \quad (20a)$$

$$\bar{\theta} \geq 0, \quad k_i = b_i + A_i x_{eq}, \quad (20b)$$

• represents block matrix terms that can be deduced from symmetry, \aleph_θ is the linear annihilator of θ , Q_a is a given basis for the null space of C_a , L is a matrix to be determined with the dimensions of $C_b(\theta)'$. The closed-loop dynamics (16) is globally asymptotically stable with the switching rule (15) and

$$V(e(t)) = \max_{i \in \mathcal{M}} \{v_i(e(t))\} \quad (21)$$

is a Lyapunov function for the system, which guarantees Lyapunov-based stability.

A. Uncertain systems

The switched control technique can be extended to uncertain parameters of the system, as proposed in [13], by considering a polytope with vertices $\{\rho_1, \dots, \rho_{2^d}\}$ for each uncertainty δ . Assuming the desired x_{eq} does not depend on δ , the closed-loop dynamics (16) becomes

$$\dot{e}(t) = \sum_{i=1}^m \theta_i(e(t)) (A_i(\delta) e(t) + k_i(\delta)). \quad (22)$$

The standard convexity properties of the LMIs are held assuming $A_i(\delta)$ and $k_i(\delta)$ are affine functions of δ , nevertheless the switched system (22), now uncertain, is globally asymptotically stable for all uncertainties in the polytope if the LMIs are feasible $\forall \delta \in \{\rho_1, \dots, \rho_{2^d}\}$ and $i \in \mathcal{M}$ [13].

IV. EXTENSIONS FOR POWER FACTOR CORRECTION

As the operation of the TPBR can be divided in $v_{in} > 0$ (Modes 1 and 2) and $v_{in} < 0$ (Modes 3 and 4), the control problem can be approached separately for each sign of the input voltage. To avoid the need of obtaining $\bar{\theta}$, which is usually not feasible for this type of converter, all P_i is considered equal within each case, $P_i := P_0 \in \mathbb{R}^{n \times n}$, $i \in \mathcal{M}$. Also, in order to avoid the inclusion of $\sum_{i=1}^m \bar{S} = 0$ in the LMIs, which would also require to obtain θ , $v_i(e(t))$ may be changed from (15) to

$$v_i(e(t)) = e(t)'P_0e(t) + 2e(t)'(S_i - \bar{S}), \quad (23)$$

which makes \bar{S} equal for all modes of each case. With the considerations stated above, knowing that only the terms that vary between modes are relevant to the switching, the switching law becomes

$$\sigma(e(t)) = \arg \max_{i \in \mathcal{M}} \{v_i(e(t))\} = \arg \max_{i \in \mathcal{M}} \{e(t)'S_i\}. \quad (24)$$

Nevertheless, the LMI problem (17) can be solved, for this case, as

$$\begin{cases} P_0 > 0; \\ Q'_a(\Psi + \Phi + LC_b(\theta) + C_b(\theta)'L')Q_a < 0, \end{cases} \quad (25)$$

where the following terms differ from (19):

$$C_b(\theta) = [\kappa_\theta \otimes I_n \quad 0_{rn \times m}], \quad (26)$$

$$\Psi = \begin{bmatrix} A'P + P'A & P'K + A'S \\ K'P + S'A & K'S + S'K \end{bmatrix}, \quad (27)$$

$$\Phi = \begin{bmatrix} 0_{rn^2 \times rn^2} & 2\alpha'S \\ 2S'\alpha & 0_{m \times m} \end{bmatrix}. \quad (28)$$

With predefined values of maximum and minimum power for nominal operation, the load resistance can be taken into account as an uncertainty δ with the vertices of the polytope defined with R_L^{min} and R_L^{max} . For power factor correction, the inductor's current i_{L_B} must be controlled to have the same waveform of the input voltage v_{in} . That includes a new uncertainty to the LMIs allowing robustness for the whole range of i_{L_B} , defining the vertices of a polytope as: when $v_{in} > 0$, vertices are

$$i_{L_B} = 0 \quad \text{and} \quad i_{L_B} = \sqrt{2} \frac{P_o^{max}}{V_{in}^{rms}}, \quad (29)$$

where P_o^{max} is the maximum output power of the converter and V_{in}^{rms} is the Root Mean Square (RMS) value of the minimum input voltage; and when $v_{in} < 0$, vertices are

$$i_{L_B} = 0 \quad \text{and} \quad i_{L_B} = -\sqrt{2} \frac{P_o^{max}}{V_{in}^{rms}}. \quad (30)$$

TABLE II: Parameters of the simulated TPBR.

Parameter	Description	Value
$V_{in}^{rms,max}$	Maximum RMS input voltage	250 V
V_{in}^{rms}	Nominal RMS input voltage	120 V
f_r	Line frequency	60 Hz
L_B	Boost inductance	2.4 mH
R_B	Boost inductor resistance	0.42 Ω
P_o^{min}	Minimum output power	25 W
P_o^{max}	Maximum output power	300 W
V_o	Output voltage	380 V
C_o	Output capacitance	270 μ F
f_s	Switching frequency considered for design	64.8 kHz

V. SIMULATION RESULTS

The TPBR was simulated in Simulink® with nonideal components, with parameters shown in Table II, which were designed for the use of the converter for an inverter refrigerator [10]. The obtained solution S_i for the LMI problem (25) considering such specification, an $\alpha_i = 10000$, $\forall i \in \mathcal{M}$, is

$$S_1 = \begin{bmatrix} -0.2951 \\ -0.0060 \end{bmatrix} \times 10^{-5}, \quad S_2 = \begin{bmatrix} 0.5417 \\ 0.0000 \end{bmatrix} \times 10^{-8}, \quad (31a)$$

$$S_3 = \begin{bmatrix} 0.3672 \\ -0.0075 \end{bmatrix} \times 10^{-5}, \quad S_4 = \begin{bmatrix} -0.5841 \\ 0.0000 \end{bmatrix} \times 10^{-8}, \quad (31b)$$

which was implemented in simulation according to (24). Harmonic content was added to the input voltage altogether with white noise, in order to almost reach the THD limit of IEEE 519 [19] for grid voltage (8 %). This way, the controller is tested at the worst case scenario in terms of input voltage.

As the current reference signal is, in practice, generated with a Digital Signal Processor (DSP), two main options, in this case, should be considered for the reference signal: i) voltage's waveform - by sensing the input voltage and using its waveform as reference signal for the inductor's current, the power factor of the converter would be at its maximum. The downside is that the harmonic content of the input voltage would be inherited by the controlled input current, increasing its THD; ii) pure sinusoidal waveform - generating a pure sinusoidal signal for the current reference eliminates the need of sensing the whole waveform of the input voltage, only needing to measure its polarity. The obtained THD will be lower for this case. As input voltage and input current waveforms may differ, nonactive power will be present in the system. Therefore, the lower the distortion in the input voltage, the higher will be the obtained power factor.

Using the input voltage waveform as reference for the controller, regarding inductor's current, the vertices of the polytope were tested. Fig. 3a and 4a shows the inductor's current i_{L_B} , input voltage v_{in} and output voltage v_o waveforms for $V_{in}^{rms} = 85$ V and output power P_o of 25 and 300 W, respectively. Whilst, Fig. 3b and 4b shows i_{L_B} , v_{in} and v_o for 250 V of input (rms) and $P_o = 25$ and 300 W, respectively. The lower the output current, the greater will be the harmonic distortion in the input current waveform, which is

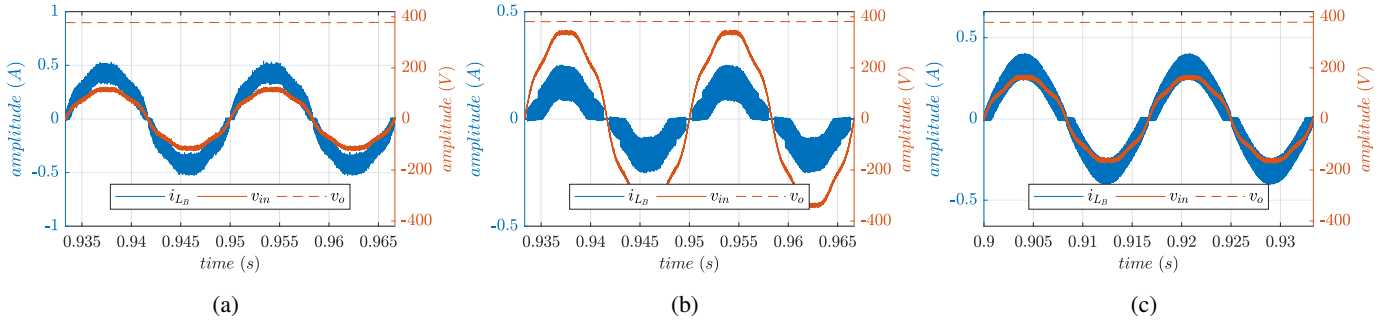


Fig. 3: i_{L_B} , v_{in} and v_o for $P_o = 25$ W with: (a) $V_{in}^{rms} = 85$ V and input voltage waveform as current reference; (b) $V_{in}^{rms} = 250$ V and input voltage waveform as current reference; and (c) $V_{in}^{rms} = 120$ V and a pure sinusoidal current reference.

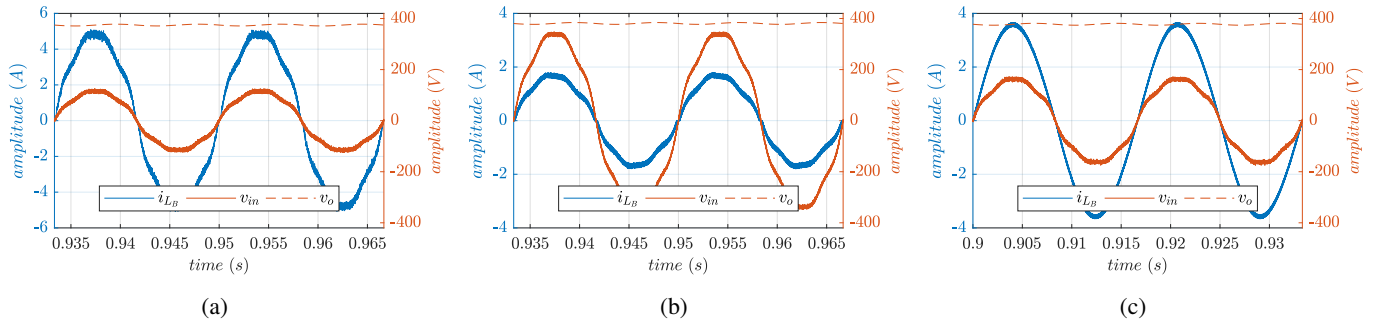


Fig. 4: i_{L_B} , v_{in} and v_o for $P_o = 300$ W with: (a) $V_{in}^{rms} = 85$ V and input voltage waveform as current reference; (b) $V_{in}^{rms} = 250$ V and input voltage waveform as current reference; and (c) $V_{in}^{rms} = 120$ V and a pure sinusoidal current reference.

a common behavior in PFC applications. Higher input voltage also results in higher THD in i_{L_B} . Note that when the input current is close to the zero value, which can be more clearly seen in Fig. 3a and 3b, the ripple at the current's waveform is enough to touch the zero value, making the converter operate for a brief period of time in DCM. This phenomenon does not affect the switched control, since its range of operation regarding input current, see (29) and (30), already includes the zero value.

Fig. 5 shows the input voltage, inductor's current and output voltage for P_o^{max} with a load step to half of P_o^{max} occurring at 0.854 seconds, the peak of the input current, with nominal input voltage V_{in}^{rms} and distorted current reference waveform. No instability occurs during the load step, as it is included within the considered polytope in the LMIs, showing controller robustness. The controller's response is fast for both i_{L_B} and v_o .

As aforementioned, the harmonic content of the input voltage waveform is inherited by the input current if its waveform is used as reference, increasing the current's THD. To demonstrate the reference following performance of the controller for another reference signal, a pure sinusoidal reference was applied to the controller. The input voltage is still distorted with harmonic content and corrupted by white noise, to the limits of IEEE 519. Two cases at the rated input voltage

(120 V) are shown in Fig. 3c and Fig. 4c, for 25 and 300 W of output power respectively. As expected, the proposed technique can achieve a very precise reference following, lowering the THD and still maintaining high power factor.

Fig. 6 shows the values of total harmonic distortion of the inductor's current i_{L_B} waveform for a pure sinusoidal reference. In comparison with values obtained in the literature [10], it shows a significant improvement. The THD results confirm what is seen in Fig. 3a, 4a, 3b and 4b: a higher THD for lower output current and for higher input voltage.

As the converter with specifications presented in Table II is designed for the application of household refrigerators, the normative energy quality requirements of IEC 61000-3-2 [20] and JIS C 61000-3-2 [21] are Class D. The presented solution for power factor correction with switched control is able to meet these requirements. The normative evaluate the THD at rated power, but switched control can obtain low THD at light load as well, which is a desired feature for household applications.

VI. CONCLUSION

Switched control is a nonlinear control technique that, after designed, can be used in an offline fashion with low computational complexity, as it is applied in a digital signal processor device through linear matrices operations. This pa-

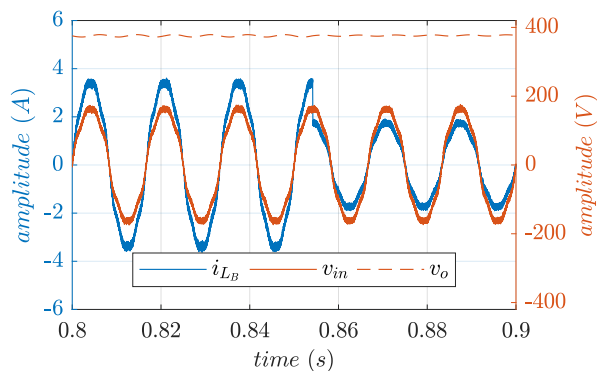


Fig. 5: Input voltage, inductor's current, and output voltage with a load step of half load at 0.854 seconds with the input voltage waveform as current reference.

per adapted switched control's theory to be applied for power factor correction in a Totem-Pole Bridgeless Rectifier.

The technique was applied through simulations in Simulink® with nonideal components and distorted input voltage, in a converter designed for household refrigeration with 300 W of nominal output power and input voltages from 85 to 250 V (rms). The results presented very low total harmonic distortion for all tested cases and a fast and stable response for a load step from 100 to 50 % of load current. As the current reference waveform can be defined by the user through a DSP in practical applications, two current references were tested: the input voltage waveform; and a pure sinusoidal waveform. Using the input voltage waveform as current reference, the converter achieves maximum power factor, whilst for a pure sinusoidal current reference, it is possible to reduce the total harmonic distortion.

As for a future works, it is suggested the application of this technique in a real prototype and its extension for partial measurement of the inductor's current. The latter should allow the user to measure a partial current at a low-side shunt resistor included between the output voltage's ground and the rectifier bridge formed by the diodes and transistors, reducing the cost of the sensors in the converter.

REFERENCES

- [1] J. Salmon, "Circuit topologies for pwm boost rectifiers operated from 1-phase and 3-phase ac supplies and using either single or split dc rail voltage outputs," in *Proceedings of 1995 IEEE Applied Power Electronics Conference and Exposition - APEC'95*, vol. 1, 1995, pp. 473–479 vol.1.
- [2] L. Huber, Y. Jang, and M. M. Jovanovic, "Performance evaluation of bridgeless pfc boost rectifiers," *IEEE Transactions on Power Electronics*, vol. 23, no. 3, pp. 1381–1390, 2008.
- [3] W. Wu, "1.5 kw digital totem pole pfc design for air-conditioner and performance comparison using igbt, sic and gan," in *PCIM Europe 2017; International Exhibition and Conference for Power Electronics, Intelligent Motion, Renewable Energy and Energy Management*, 2017, pp. 1–5.
- [4] K. Zhu, M. O'Grady, J. Dodge, J. Bendel, and J. Hostetler, "1.5 kw single phase ccm totem-pole pfc using 650v sic cascodes," in *2016 IEEE 4th Workshop on Wide Bandgap Power Devices and Applications (WiPDA)*, 2016, pp. 90–94.

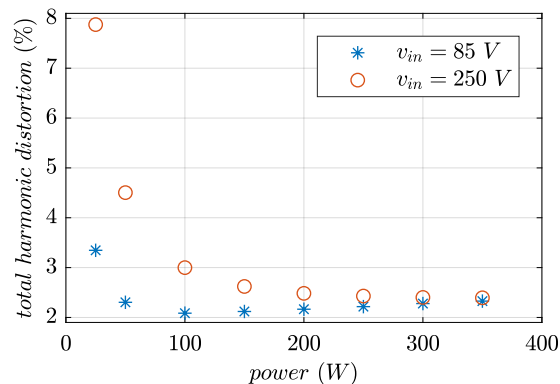


Fig. 6: Total harmonic distortion obtained for $v_{in} = 85$ V and $v_{in} = 250$ V with a pure sinusoidal current reference for different output power values.

- [5] R. Zhang, S. Liu, B. Li, N. Zhao, G. Wang, and D. Xu, "Totem-pole bridgeless boost pfc converter based on gan hemt for air conditioning applications," in *2018 2nd IEEE Conference on Energy Internet and Energy System Integration (EI2)*, 2018, pp. 1–9.
- [6] P. C. Todd, "Uc3854 controlled power factor correction circuit design," Unintode Application Note U-134, Texas Instruments, pp. 3–269, 3–288.
- [7] S. Buso, P. Mattavelli, L. Rossetto, and G. Spiazzi, "Simple digital control improving dynamic performance of power factor preregulators," *IEEE Transactions on Power Electronics*, vol. 13, no. 5, pp. 814–823, 1998.
- [8] Z. Lai and K. Smedley, "A family of continuous-conduction-mode power-factor-correction controllers based on the general pulse-width modulator," *IEEE Transactions on Power Electronics*, vol. 13, no. 3, pp. 501–510, 1998.
- [9] R. Brown and M. Soldano, "One cycle control ic simplifies pfc designs," in *Twentieth Annual IEEE Applied Power Electronics Conference and Exposition, 2005. APEC 2005.*, vol. 2, 2005, pp. 825–829 Vol. 2.
- [10] G. d. S. Fischer, C. Rech, and Y. R. de Novaes, "Extensions of leading-edge modulated one-cycle control for totem-pole bridgeless rectifiers," *IEEE Transactions on Power Electronics*, vol. 35, no. 5, pp. 5447–5460, 2020.
- [11] M. Branicky, "Multiple lyapunov functions and other analysis tools for switched and hybrid systems," *IEEE Transactions on Automatic Control*, vol. 43, no. 4, pp. 475–482, 1998.
- [12] P. Colaneri, J. C. Geromel, and A. Astolfi, "Stabilization of continuous-time switched nonlinear systems," *Systems & Control Letters*, vol. 57, no. 1, pp. 95–103, 2008. [Online]. Available: <https://www.sciencedirect.com/science/article/pii/S0167691107000953>
- [13] A. Trofino, D. Assmann, C. C. Scharlau, and D. Coutinho, "Switching rule design for switched dynamic systems with affine vector fields," *Proceedings of the 48th IEEE Conference on Decision and Control (CDC) held jointly with 2009 28th Chinese Control Conference*, pp. 6365–6370, 2009.
- [14] A. Trofino, C. C. Scharlau, T. J. Dezuio, and M. C. de Oliveira, "Stabilizing switching rule design for affine switched systems," in *2011 50th IEEE Conference on Decision and Control and European Control Conference*, 2011, pp. 1183–1188.
- [15] G. Battistelli, D. Selvi, and A. Tesi, "Robust switching control: Stability analysis and application to active disturbance attenuation," *IEEE Transactions on Automatic Control*, vol. 62, no. 12, pp. 6369–6376, 2017.
- [16] A. Trofino, C. C. Scharlau, T. J. Dezuio, and M. C. de Oliveira, "Switching rule design for affine switched systems with \mathcal{H}_∞ performance," in *2012 IEEE 51st IEEE Conference on Decision and Control (CDC)*, 2012, pp. 1923–1928.
- [17] D. Van de Sype, K. De Gussemme, A. Van den Bossche, and J. Melkebeek, "A sampling algorithm for digitally controlled boost pfc converters," *IEEE Transactions on Power Electronics*, vol. 19, no. 3, pp. 649–657, 2004.
- [18] B. Lu, R. Brown, and M. Soldano, "Bridgeless pfc implementation using

one cycle control technique,” in *Twentieth Annual IEEE Applied Power Electronics Conference and Exposition, 2005. APEC 2005.*, vol. 2, 2005, pp. 812–817 Vol. 2.

- [19] “Ieee recommended practice and requirements for harmonic control in electric power systems,” Institute of Electrical and Electronics Engineers, New York, United States of America, Standard, 2018.
- [20] “Electromagnetic compatibility (emc) - part 3-2: Limits - limits for harmonic current emissions (equipment input current $I_n \leq 16$ a per phase),” International Electrotechnical Commission, Geneva, Switzerland, Standard, 2018.
- [21] “Electromagnetic compatibility (emc) part 3-2: Limits - limits for harmonic current emissions (equipment input current $I_n \leq 20$ a per phase),” Japanese Standards Association, Tokyo, Japan, Standard, 2011.